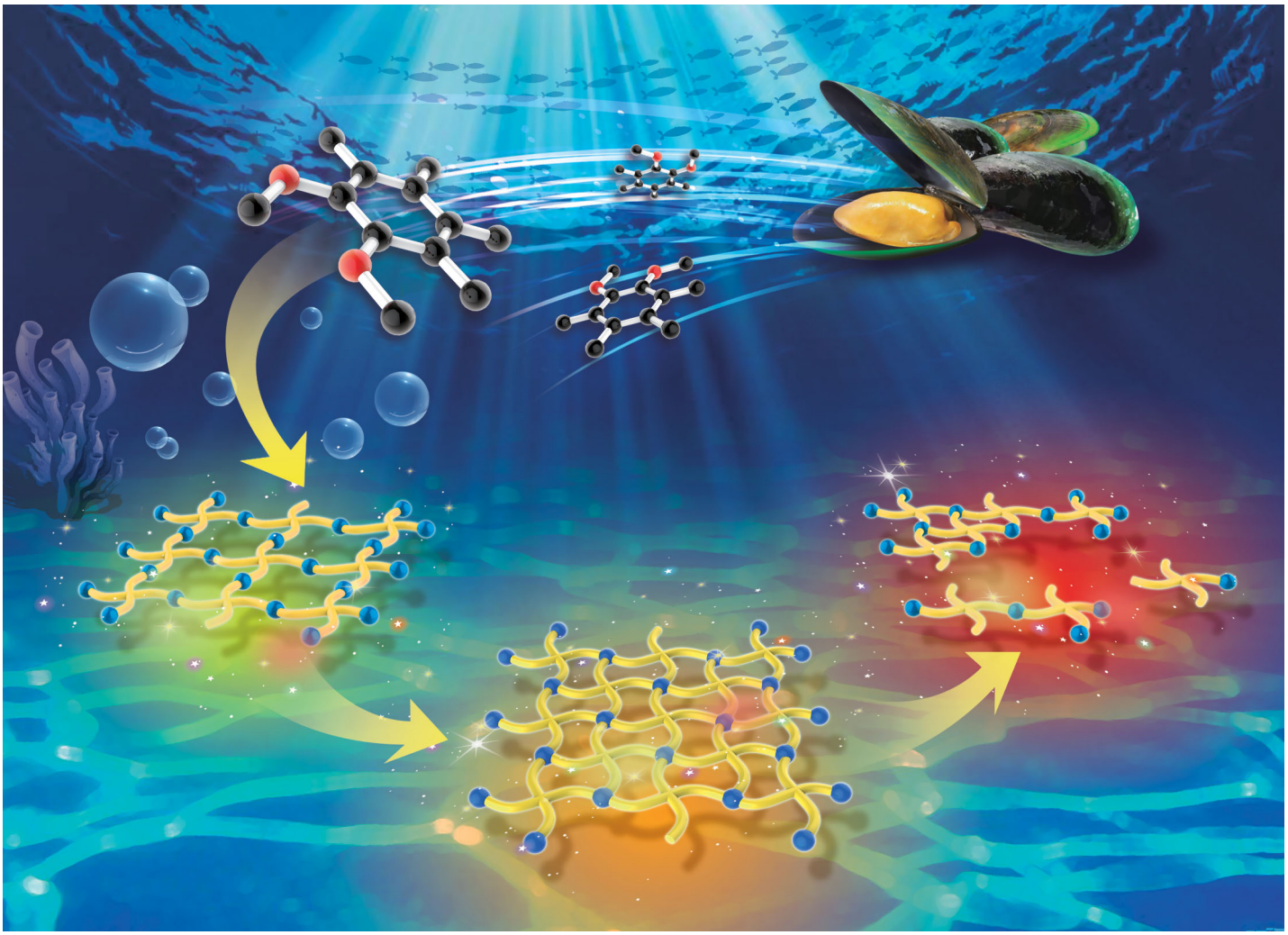

Showcasing research from the laboratory of Wei Sun, Tsinghua-Berkeley Shenzhen Institute, Tsinghua University, China.

The multifaceted nature of catechol chemistry: bioinspired pH-initiated hyaluronic acid hydrogels with tunable cohesive and adhesive properties

By regulating pH, a series of bioinspired, pH-initiated hyaluronic acid hydrogels that possess tunable cohesive and adhesive properties was developed based on catechol-related chemistry.

As featured in:

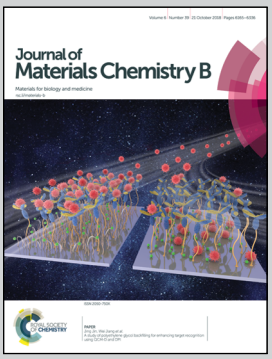

See Shengli Mi, Wei Sun *et al.*, *J. Mater. Chem. B*, 2018, **6**, 6234.

ROYAL SOCIETY OF CHEMISTRY

rsc.li/materials-b

Registered charity number: 207890

Journal of Materials Chemistry B

PAPER

View Article Online
View Journal | View Issue

Cite this: J. Mater. Chem. B, 2018, 6, 6234

The multifaceted nature of catechol chemistry: bioinspired pH-initiated hyaluronic acid hydrogels with tunable cohesive and adhesive properties†

Zhongwei Guo, [ab] Shengli Mi *[b] and Wei Sun*[abcd]

Received 8th July 2018,
Accepted 3rd September 2018

DOI: 10.1039/c8tb01776j

rsc.li/materials-b

The field of hydrogels has rapidly expanded in recent years. A growing theme is the development of hydrogels that are bioinspired, with tailorable physicochemical properties. Marine mussels utilize their byssus to adhere themselves to rocks and thereby decrease the turbulent buffeting of the intertidal zone. An increase in pH is a noticeable phenomenon during the mussel byssus secretion and formation processes. In this study, by mimicking the acidic-to-basic pH switch that occurs during byssus formation, a series of bioinspired, pH-initiated hyaluronic acid (HA) hydrogels that possess tunable cohesive and adhesive properties were developed. Specifically, four different kinds of hyaluronic acid (HA) hydrogel crosslinking networks were fabricated by utilizing the multifaceted nature of catechol chemistry, including metal–catechol coordination, quinone–catechol dismutation, quinone–amine Michael addition and Schiff base reactions, or quinone–thiol Michael addition reactions. Our research demonstrated that pH, as one of the most important environmental variables for mussels, plays a vital role in regulating the cohesion and adhesion behaviors. And regarding the development of new materials, this biomimetic strategy also demonstrates alternative and tunable crosslinking approaches that can overcome the limitations of current HA hydrogels.

1. Introduction

In nature, there are many outstanding phenomena from which material scientists can acquire inspiration to design and fabricate new materials.[1,2] Marine mussels, for instance, utilize their byssus to adhere themselves to rocks and thereby decrease the turbulent buffeting of the intertidal zone. To better mimic mussel byssus formation and functions, increasing efforts have been devoted to elucidate the crosslinking mechanism of mussel byssus.[3–8] The most direct way is to use byssus itself as a research object, which is mainly composed of mussel foot proteins (mfps). However, tedious extraction procedures and limited quantities make the extensive use of these natural mussel foot proteins unlikely.[8–10] And the complex composition of mussel foot proteins cannot be easily controlled to meet the requirements for practical applications, thus stimulating the growth of mussel-inspired synthetic materials.[11–16]

Hyaluronic acid (HA), an essential component of the ECM, is one of nature's most versatile and fascinating polymers and has been widely utilized as a biocompatible and biodegradable material for tissue engineering. HA can be easily functionalized with various crosslinking agents *via* its hydroxyl or carboxyl groups to fabricate hydrogels, which are promising candidates as tissue-engineered scaffolds for biomedical applications.[17–19] However, currently available HA hydrogels still have some limitations. For instance, existing modifications and crosslinking approaches often lead to the limited adhesive property of HA hydrogels. Moreover, the uncontrollable gelation process and the lack of responses to stimuli have resulted in many limitations for potential clinical applications.[19–21] Therefore, an alternative crosslinking strategy is required to produce highly adhesive and property-tailorable HA hydrogels.

The field of hydrogels has rapidly developed in recent years. A growing theme is the development of hydrogels that are bioinspired, with tailorable physicochemical properties.[22–28] In this study, by mimicking the acidic-to-basic pH switch that occurs during byssus formation, a novel series of bioinspired, pH-initiated HA hydrogels that possess tunable cohesive and adhesive properties were developed. We believe that these pH-initiated HA crosslinking networks may be useful for the

[a] Precision Medicine and Healthcare Research Center, Tsinghua-Berkeley Shenzhen Institute, Shenzhen, China. E-mail: weisun@mail.tsinghua.edu.cn
[b] Biomanufacturing Engineering Laboratory, Graduate School at Shenzhen, Tsinghua University, Shenzhen, China
[c] Department of Mechanical Engineering and Mechanics, Tsinghua University, Beijing, China
[d] Department of Mechanical Engineering, Drexel University, Philadelphia, PA, USA

† Electronic supplementary information (ESI) available. See DOI: 10.1039/c8tb01776j

fabrication of new biomaterials and shed some light on the clarification of mussel byssus formation.

2. Results and discussion

2.1 Synthesis and characterization of HA-Cat, HA-SH and HA-NH_2

Unlike the complex composition of mussel foot proteins, mussel-inspired synthetic materials always possess specific molecular choices that one can control and modify. From the perspective of composition, the mussel byssus features a range of proteins, such as mfp-3, mfp-5 and mfp-6. All of these mfp families share a common feature: the presence of a distinctive catecholic amino acid, 3,4-dihydroxy-L-phenylalanine (DOPA). In addition to the common catechol group, lysine (amine group) and cysteine (thiol group) also exist.[8–10] To simulate and clarify the gelation strategy of mussel byssus, hyaluronic acid was functionalized with catechols, amines and thiols, respectively.

HA-Cat, a catechol-modified linear polymer, was synthesized by an EDC/NHS coupling reaction, which conjugates the carboxylic acid group of HA with the amine group of dopamine. Scheme S1a (ESI†) illustrates the synthetic route to HA-Cat. The successful introduction of catechol groups was confirmed by the appearance of peaks at approximately 7.0 ppm in its ^{1}H-NMR spectra (Fig. 1b). The substitution degree was calculated based on the ^{1}H-NMR spectrum of HA-Cat. In this reaction, the molar ratio of reactants was HA : EDC : NHS : dopamine = 1 : 1 : 1 : 1, 1 : 2 : 2 : 2 and 1 : 3 : 3 : 3, which resulted in the corresponding catechol-modification ratios in HA-Cat of 26%, 35% and 43%, respectively.

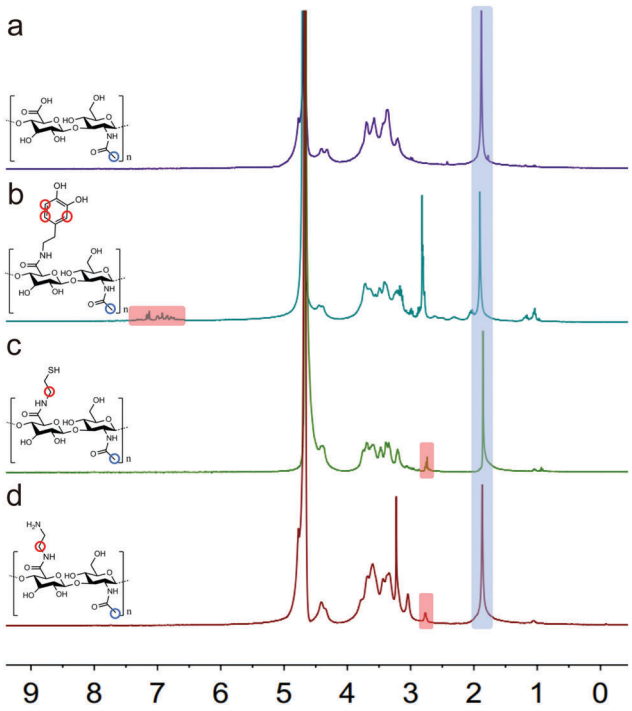

Fig. 1 ^{1}H-NMR spectra of HA (a); HA-Cat (b); HA-SH (c); HA-NH_2 (d).

HA-SH, a thiol-modified linear polymer, was synthesized by a simple two-step reaction. Scheme S1b (ESI†) illustrates the synthetic route to HA-SH. First, the carboxyl groups of HA were chemically activated by EDC and HOBt and then connected with cystamine. Second, DTT was used to reduce the disulfide bonds to obtain HA-SH. The successful introduction of thiol groups was confirmed by the appearance of peaks at approximately 2.7 ppm (NH-**CH_2**-CH_2-SH) in its ^{1}H-NMR spectra (Fig. 1c). The thiol-modification ratio of HA-SH was approximately 21%, as determined from the ^{1}H-NMR data.

HA-NH_2, an amine-modified linear polymer, is synthesized by an EDC/HOBt coupling reaction, which conjugates the carboxylic acid group of HA with the amine group of ethylenediamine. Scheme S1c (ESI†) illustrates the synthetic route to HA-NH_2. The successful introduction of amine groups was confirmed by the appearance of peaks at approximately 2.7 ppm (NH-**CH_2**-CH_2-NH_2) in its ^{1}H-NMR spectra (Fig. 1d). The amine-modification ratio of HA-NH_2 was approximately 27%, as determined from the ^{1}H-NMR data.

2.2 Properties of Fe^{3+}-induced HA-Cat hydrogels: influence of pH

Mussel byssus is rich in catechol-containing proteins and inorganic elements such as Fe^{3+}. The interaction between Fe^{3+} and the catechol moieties has long been correlated with the formation and function of mussel byssus.[3,29–32] To further elucidate the links between pH, Fe^{3+} and catechol groups, a series of Fe^{3+}-induced HA-Cat hydrogels possessing different colors, gelation rates and mechanical properties were fabricated by regulating pH. As shown in Fig. S1 and S2 (ESI†), a Fe^{3+} : catechol molar ratio of 1 : 3 was selected as the optimum and used in the subsequent research, due to its higher storage modulus than other ratios. As shown in Fig. 2a, the addition of Fe^{3+} into the HA-Cat solution initiated an instant gelation process, which resulted in a yellow elastic hydrogel (pH: 1–2). By increasing the pH of the pre-gel mixtures, the hydrogel color changed from green (pH: 3–4) to dark green (pH: 4–5), purple (pH: 6–7), purple red (7–8) and brown red (pH: 9–10). No gelation process was observed by increasing the pH of the HA-Cat solution alone. Previous studies have already suggested that the appearance of different colors represents unique crosslinking mechanisms.[32] UV-Vis spectra were utilized to clarify the internal crosslinking mechanism underlying these color variations (Fig. 3a and 4a). Only the peaks above 350 nm were used because the data below this range were too severely affected by overlapping. Only one narrow absorption peak at 400 nm emerged when the gel pH was strongly acidic (pH: 2.0). This result suggests that the addition of Fe^{3+} could induce the oxidation of catechol into quinone (λ_{max} = 400 nm), which initiates covalent crosslinking.[24,31,32] Upon increasing the pH (pH: 3.0), a similar absorption peak was also observed at 400 nm, but a new broad absorption peak appeared at 730 nm. These results indicated that Fe^{3+} could induce the oxidation of the catechol moiety into quinone, as well as the coordination with catechols (primarily a mono-complex at pH 3.0). In addition, EDTA was used to disintegrate the coordination bonds between Fe^{3+} and catechols, which caused the green gel to turn into a light

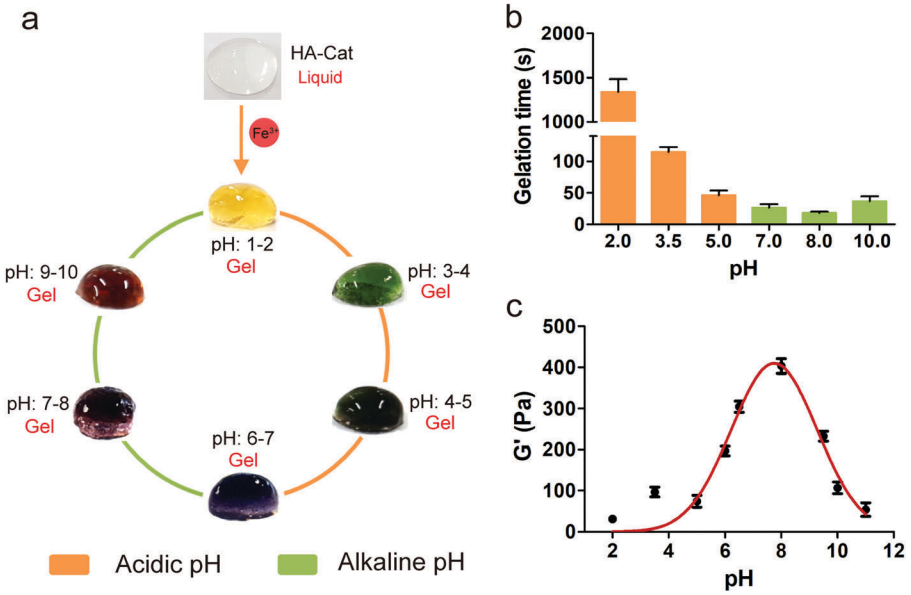

Fig. 2 The preparation and characterization of pH-initiated Fe^{3+}-induced HA-Cat hydrogels (Fe^{3+} : catechol molar ratio of 1 : 3). A schematic representation of the hydrogel formation over the entire pH range, including the physical state and color variation (a); gelation time of the hydrogel at various pH (b); storage modulus (G') of the hydrogel plotted as a function of pH for a strain of 5% and a frequency of 1 Hz (c).

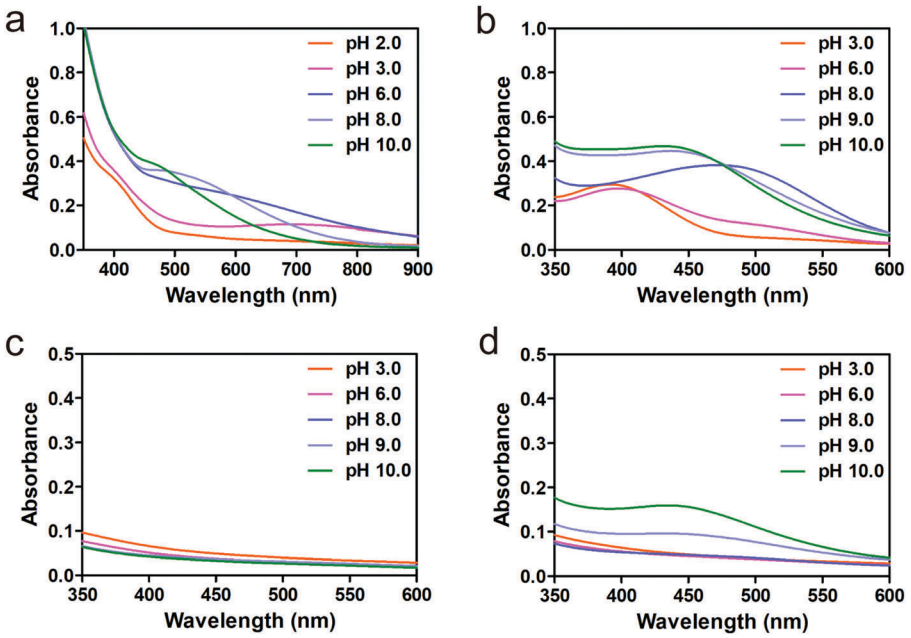

Fig. 3 UV-Vis spectra of Fe^{3+}-induced HA-Cat solution (a), $NaIO_4$-induced HA-Cat solution (b), HA-Cat & HA-SH solution (c), HA-Cat & HA-NH_2 solution (d) with increasing pH values.

yellow gel (Fig. S3, ESI†). This process is also illustrated by the decrease in the mechanical strength and the disappearance of the absorption peak at 730 nm (Fig. S4, ESI†).[31] By regulating gel pH from acidic to basic conditions, the UV-Vis absorption peak shifted to 490 nm, which indicates that the Fe^{3+}–catechol coordination bond changed from mono-complex (730 nm, pH: 3.0) to tris-complex (490 nm, pH: 10.0).[32]

More than just color variation occurs, changes in the internal crosslinking mechanism induced by a pH change also have a significant impact on the gelation time and the mechanical properties of hydrogels. As shown in Fig. 2b, the gelation time was nearly 1200 s when the pre-gel solution pH was adjusted to pH 2.0. By increasing the pre-gel solution pH, the gelation time decreased dramatically to 140 s (pH: 3.5), 25 s (pH: 7.0), 15 s (pH: 8.0) and 40 s (pH: 10.0). As revealed by the UV-Vis spectra, this substantial acceleration in the gelation rate clearly benefits from the rapid formation of Fe^{3+}–catechol coordination bonds, which are highly sensitive to pH. In contrast, the fast

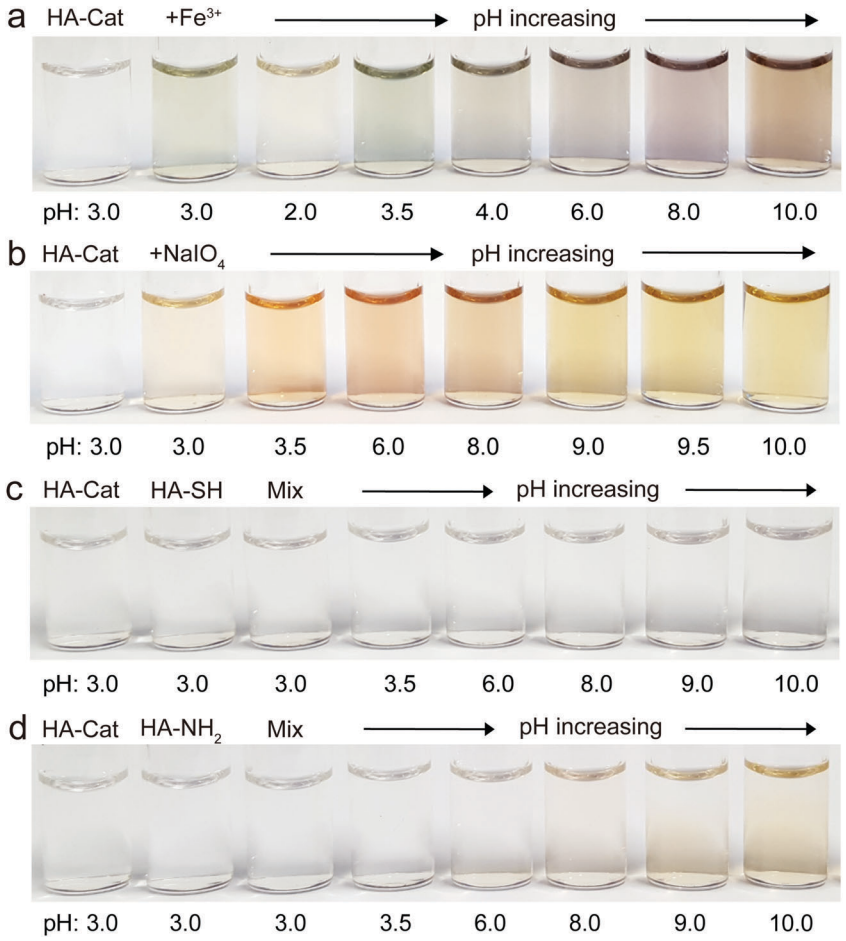

Fig. 4 The color change image of Fe^{3+}-induced HA-Cat solution (a), $NaIO_4$-induced HA-Cat solution (b), HA-Cat & HA-SH solution (c), HA-Cat & HA-NH_2 solution (d) with increasing pH values.

solidification of mussel byssus also experiences an obvious pH increase process. Therefore, it is supposed that the coordination interactions between Fe^{3+} and catechol groups play an important role in the fast solidification behavior of mussel byssus.

The impact of pH on the mechanical properties of Fe^{3+}-induced HA-Cat hydrogels was investigated by using a rheological method. Coincidentally, the storage modulus (G') of the hydrogels displayed a bell-shaped curve at different pH values, with a maximum value (G': 400 Pa, 1 Hz frequency) around the pH of seawater (pH: 8.0–8.5), as shown in Fig. 2c. Below this pH value, the storage modulus rapidly increased along with increasing pH, from 35 Pa (pH: 2.0) to 200 Pa (pH: 6.5) *via* 70 Pa (pH: 5.0). As shown in the UV-Vis spectra, this tendency was mainly attributed to the formation of Fe^{3+}–catechol coordination bonds. With increasing pH, the Fe^{3+}–catechol coordination complexes will transform from mono-complexes into bis- or tris-complexes, which endows the hydrogel with a higher mechanical strength. However, the hydrogels tended to be softer when the pH was regulated above seawater (pH: 8.0–8.5) (Scheme 1). This unexpected result was also confirmed by the oscillatory time sweep of the hydrogels (Fig. S5, ESI†), which showed an evident decline in the gel maturation rate. A possible explanation is that the instantaneous addition of a high amount of sodium hydroxide makes the local pH too high, which leads to excessive gelation inside the pre-gel system, which leads to an inhomogeneous structure. This process also makes it harder for chain rearrangement during the pre-gel solution mixing step, especially for high molecular weight hyaluronic acid.[33] All these processes will lead to inhomogeneous gelation inside the hydrogel crosslinking network, which weakens the mechanical properties.

The relationship between pH and mechanical strength (bell-shaped curve) also sheds light on how organisms can exploit a given environment (seawater pH: 8.0–8.5) to acquire the best survival ability. In general, all of the above results demonstrated that the Fe^{3+}–catechol crosslinking network is actually a pH-sensitive, dynamic, dual-crosslinking system composed of coordination bonds and covalent bonds. pH, as one of the most important environmental variables for mussels, could be utilized to trigger and regulate the cohesion behavior of the Fe^{3+}-induced HA-Cat gel system.

2.3 Properties of $NaIO_4$-induced HA-Cat hydrogels: influence of pH

Previous studies have already shown that the catechol group is susceptible to oxidation, especially at the basic pH of seawater.[31,34–36]

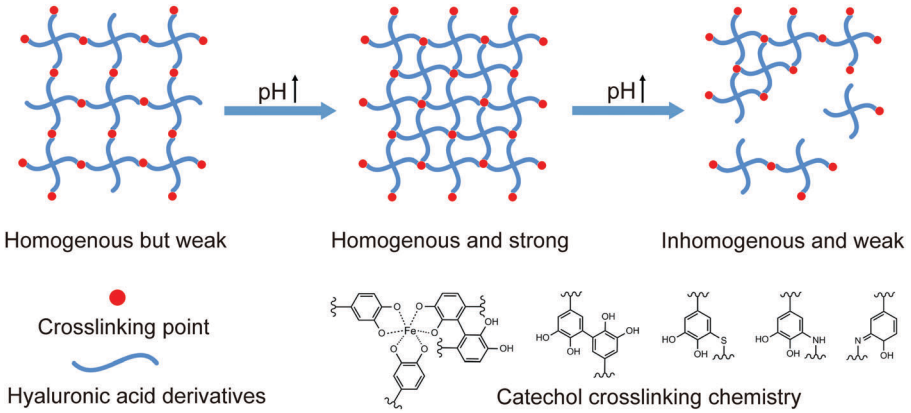

Scheme 1 pH influence on the crosslinking network of hyaluronic acid hydrogels, which is fabricated by utilizing the multifaceted nature of catechol crosslinking chemistry.

Sodium periodate is a frequently used oxidizer. To further elucidate the links between pH, oxidants and catechol groups, a series of $NaIO_4$-induced HA-Cat hydrogels were developed by regulating pH. As shown in Fig. S7 and S8 (ESI†), an IO_4^-: catechol molar ratio of 1 : 3 was selected as the optimum and used in the subsequent research, due to its higher storage modulus than other ratios. As shown in Fig. 5a, the addition of $NaIO_4$ into HA-Cat solution initiated a slow gelation process, which resulted in a light yellow (signature color of *o*-quinone, λ_{max} = 400 nm) elastic hydrogel (pH: 1–2). As the pH increased, the gel color changed from yellow (pH: 3–4) to brown (pH: 9–10).

As shown in the UV-Vis spectra, when the solution pH was maintained at pH 3.0, one absorption peak at 400 nm appeared, which represents the oxidation of catechol into reactive quinone species (Fig. 3b and 4b). Highly reactive *o*-quinone is electron deficient and prefers to react with catechol by quinone–phenol dismutation, which initiates covalent crosslinking.[34,36,37] Upon increasing the pH to 6.0, a new absorption peak was observed near 495 nm, while the peak at 400 nm slightly declined. This characteristic peak shift indicated the rearrangement process of quinone–catechol complexes. Finally, when the pH was higher than 9.0, the peaks at 400 nm and 495 nm disappeared, and a new peak emerged at 450 nm. These absorption peak transformations represent the end of the quinone–catechol rearrangement process.[37]

More than just color variation occurs, the pH increase also has a significant impact on the gelation time and the mechanical properties of hydrogels. As shown in Fig. 5b, the gelation time was nearly 2600 s when the system pH was adjusted to pH 2.0. By increasing the pre-gel solution pH, the gelation time decreased dramatically to 1900 s (pH: 3.5), 70 s (pH: 5.5), 20 s (pH: 8.0), 15 s (pH: 9.0) and 38 s (pH: 10.0). As shown in the UV-Vis spectra, this

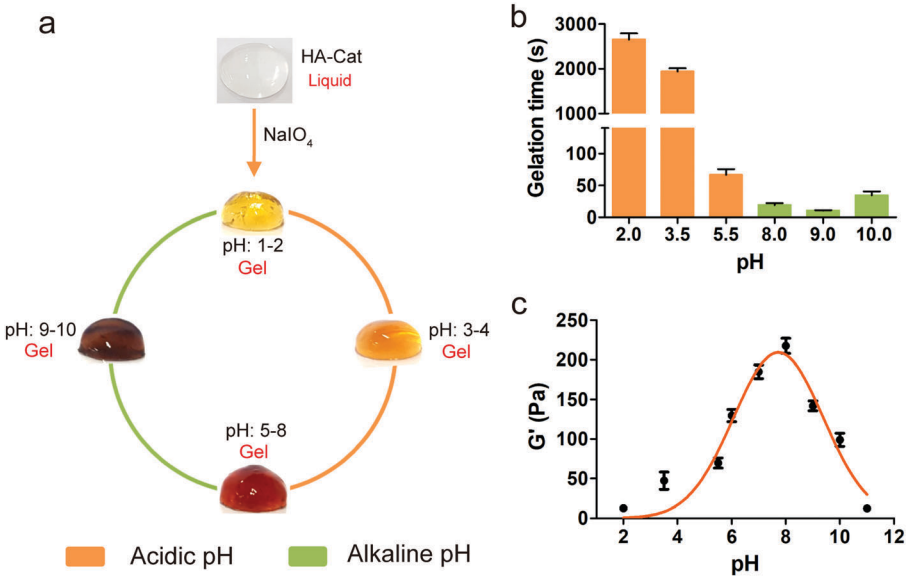

Fig. 5 The preparation and characterization of pH-initiated $NaIO_4$-induced HA-Cat hydrogels (IO_4^- : catechol molar ratio of 1 : 3). A schematic representation of the hydrogel formation over the entire pH range, including the physical state and color variation (a); gelation time of the hydrogel at various pH (b); storage modulus (G') of the hydrogel plotted as a function of pH for a strain of 5% and a frequency of 1 Hz (c).

substantial acceleration in the gelation rate clearly benefits from the rapid formation of covalent catechol–catechol bonds, which are highly sensitive to environmental pH. In contrast, the fast solidification of mussel byssus also experiences an obvious pH increase process. Therefore, it is supposed that the pH-increasing behavior initiates the pre-existing interaction of byssus catechol groups with oxidants in seawater to form a covalent crosslinking network.

The impact of pH on the mechanical properties of $NaIO_4$-induced HA-Cat hydrogels was investigated by using a rheological method. Coincidentally, the storage modulus (G') of the hydrogels also displayed a bell-shaped curve at different pH values, with a maximum storage modulus (G': 250 Pa, 1 Hz frequency) around the pH of seawater, as shown in Fig. 5c. Below this pH value, the storage modulus rapidly increased along with increasing pH, from 25 Pa (pH: 2.0) to 250 Pa (pH: 8.0) *via* 50 Pa (pH: 3.5) and 70 Pa (pH: 5.5). As revealed by the UV-Vis spectra, this tendency was mainly attributed to the formation of covalent catechol–catechol bonds. With increasing pH, more reactive quinone species emerge and crosslink with catechol groups, which endows the present system with a higher mechanical strength. However, the hydrogels tended to be softer when the pH was regulated above seawater (Scheme 1). This unexpected result was also confirmed by the oscillatory time sweep of the hydrogels (Fig. S9, ESI†), which showed an evident decline in the gel maturation rate. Similar to the Fe^{3+}-induced HA-Cat hydrogels, a pH that is too high will lead to inhomogeneous gelation inside the hydrogel crosslinking network, which weakens the mechanical properties. All of the above results demonstrated that the $NaIO_4$-induced HA-Cat crosslinking network is a pH-sensitive, covalent crosslinking system. pH could be utilized to trigger and regulate the cohesion behavior of the $NaIO_4$-induced HA-Cat gel system.

2.4 Properties of HA-Cat & HA-SH hydrogels: influence of pH

In addition to the DOPA moiety, mfp-6 also possesses a high content of cysteine.[8–10] However, the role of cysteine remains poorly understood. It is supposed that the interactions between catechol (DOPA) and thiol groups (cysteine) also play a key role in the mussel byssus formation process and byssus-related functions. By regulating pH, a series of HA-Cat & HA-SH hydrogels possessing different gelation rates and mechanical properties were fabricated. As shown in Fig. S11 and S12 (ESI†), a catechol : thiol molar ratio of 1 : 1 was selected as the optimum and used in the subsequent research, due to its higher storage modulus than other ratios.

As shown in Fig. 6a, the addition of HA-SH solution (pH: 3–4, colorless) into HA-Cat solution (pH: 3–4, colorless) did not initiate any gelation process (pH: 3–4). As the pH increased, the colorless liquid mixture (pH: 3–4) became a colorless viscous one (pH: 4–6), which was still unable to form a gel even when the time was prolonged. Only when the pH rose above neutral pH did the whole mixture turn into a stable elastic gel.

With increasing pH, the gelation time decreased dramatically from infinite time to 30 s (pH: 10.0) *via* 70 s (pH: 7.0) and 25 s (pH: 8.0) (Fig. 6b). The substantial acceleration in the gelation rate benefits from the rapid occurrence of Michael addition reactions between the thiol and reactive quinone groups, which are highly sensitive to environmental pH.[5,6] Therefore, it is supposed that the pH-increasing process also initiates the byssus pre-existing catechol group interaction with the thiol groups in mfps to form a covalent crosslinking network. No gelation process was observed by simply increasing the pH of the HA-SH solution alone. More than just gelation time variations occur, pH increases also have a significant impact on the mechanical properties of hydrogels (Fig. 6c).

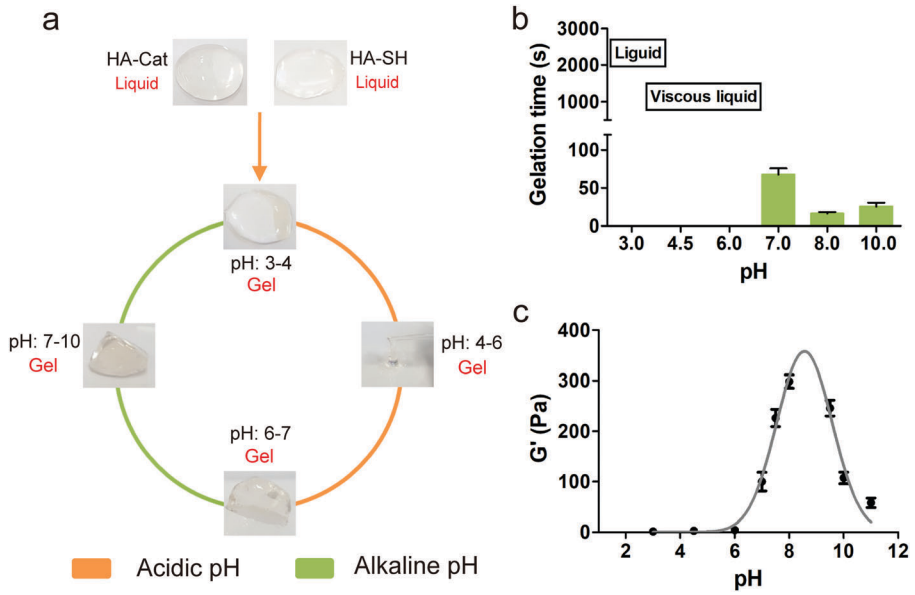

Fig. 6 The preparation and characterization of pH-initiated HA-Cat & HA-SH hydrogels (catechol : thiol molar ratio of 1 : 1). A schematic representation of gel formation over the entire pH range, including the physical state and color variation (a); gelation time of the hydrogel at various pH (b); storage modulus (G') of the hydrogel plotted as a function of pH for a strain of 5% and a frequency of 1 Hz (c).

Coincidentally, the mechanical properties of the hydrogels also displayed a bell-shaped curve at different pH values, with a maximum storage modulus (G': 340 Pa, 1 Hz frequency) around the pH of seawater (pH: 8.0–8.5). Below this pH value, the storage modulus rapidly increases along with increasing pH, since more reactive quinone species emerge and react with thiol groups, which endows the hydrogel with a higher mechanical strength (Scheme 1). However, the hydrogels tended to be softer when the pH was regulated above that of seawater (pH: 8.0–8.5). This unexpected result was also confirmed by the oscillatory time sweep of the hydrogels (Fig. S13, ESI†), which shows an evident decline in the gel maturation rate.

Previous research indicated that typical marine conditions will oxidize DOPA to initiate quinone species reactions which consequently diminish their adhesion ability. How do mussels maintain a balance between catechol and quinone species such that mussel byssus possesses cohesion and adhesion abilities simultaneously? The concurrent secretion of thiol-rich mfp-6 could be the key to this issue.[38] To illustrate this point, the UV-Vis spectra were utilized (Fig. 3c and 4c). Usually, increasing the pH values will induce catechol oxidation into a quinone moiety, which possesses a maximum absorption peak at 400 nm. However, no absorption peaks were observed at approximately 400 nm, as shown in the UV-Vis spectra (Fig. 3c). The system remained colorless from acidic to basic pH. These results all indicated that the presence of thiol groups protected the catechol group from oxidation. In general, all of the above results demonstrated that the HA-Cat & HA-SH crosslinking network is a pH-initiated, covalent crosslinking system. pH could be utilized to trigger and regulate the cohesion behavior of the HA-Cat & HA-SH gel system. Additionally, the presence of thiol groups also plays a key role in maintaining the balance between catechol and quinone species.

2.5 Properties of HA-Cat & HA-NH_2 hydrogels: influence of pH

In addition to the common catechol group, mfp-3 and mfp-5 are rich in lysine and DOPA, which are constantly in adjacent positions along the protein sequences. However, the role of lysine remains poorly understood.[8,9] In this study, a series of HA-Cat & HA-NH_2 hydrogels possessing different gelation rates and mechanical properties were fabricated by regulating the pH. As shown in Fig. S15 and S16 (ESI†), a catechol : amine molar ratio of 1 : 1 was selected as the optimum and used in the subsequent research, due to its higher storage modulus than other ratios. As shown in Fig. 7a, the addition of HA-NH_2 (pH: 3–4, colorless) into HA-Cat solution (pH: 3–4, colorless) did not initiate any visible gelation. As the pH increased, the colorless liquid mixture (pH: 3–4) turned into a light brown viscous one (pH: 5–7), which was unable to form a gel even prolonging the time. Only when the pH rose above neutral pH did the whole mixture turn into a stable elastic gel (pH: 7–10). This process is similar to the HA-Cat & HA-SH hydrogel because the crosslinking reaction begins with the induction of quinone species by increasing pH. No gelation was observed by simply increasing the pH of the HA-NH_2 solution alone.

With increasing pH, the gelation time decreased from infinite time to 2350 s (pH: 10.0) *via* 3000 s (pH: 7.0) and 1700 s (pH: 8.0) (Fig. 7b). The crosslinking reaction is derived from the occurrence of Michael addition reactions or Schiff base reactions between amine and catechol groups, which are highly sensitive to the solution pH.[5,28,37] As shown in the UV-Vis spectra, the increasing pH values caused catechol–amine reactions (Fig. 3d and 4d). However, the gelation rate

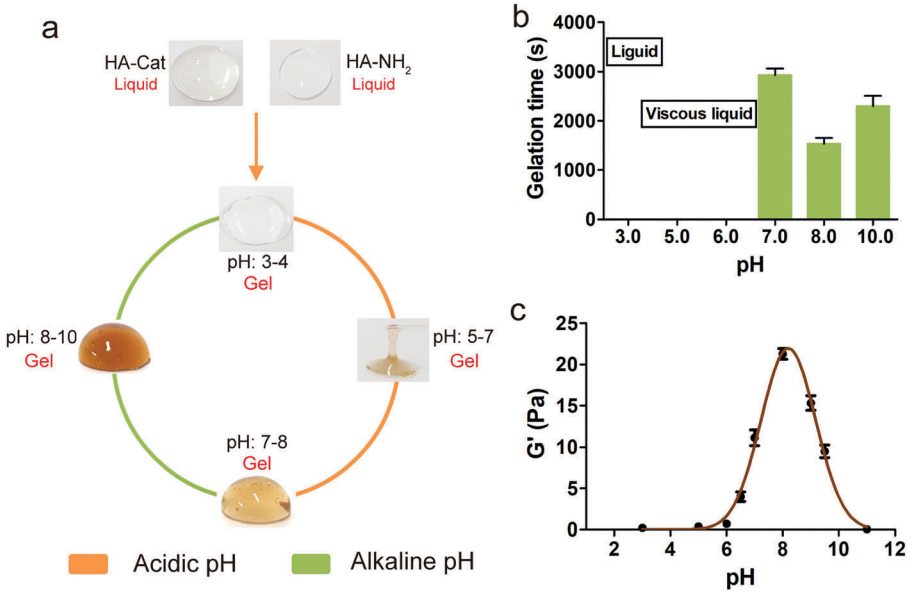

Fig. 7 The preparation and characterization of pH-initiated HA-Cat & HA-NH_2 hydrogels (catechol : amine molar ratio of 1 : 1). A schematic representation of gel formation over the entire pH range, including the physical state and color variation (a); gelation time of the hydrogel at various pH (b); storage modulus (G') of the hydrogel plotted as a function of pH for a strain of 5% and a frequency of 1 Hz (c).

was very slow compared with that of the other pH-initiated HA-Cat & HA-SH crosslinking hydrogels, which could be related to the different kinetics of catechol oxidation chemistry. Specifically, the reaction between quinone species and thiol groups is one of the most favorable reactions and is approximately 50 000 times faster than quinone–amine reactions.[39] More than just gelation time variations occur, pH increases also have a significant impact on the mechanical properties of hydrogels (Fig. 7c). The mechanical properties of the hydrogels displayed a bell-shaped curve at different pH values, with a maximum storage modulus (G': 25 Pa, 1 Hz frequency) around the pH of seawater (pH: 8.0–8.5). In general, all of the above results demonstrated that the HA-Cat & HA-NH_2 crosslinking network is a pH-initiated, covalent crosslinking system. pH could be utilized to trigger and regulate the cohesion behavior of the HA-Cat & HA-NH_2 gel system. However, the cohesion ability of this system is weak due to its inferior reaction kinetics.

2.6 pH influence on the morphological changes of different hydrogels

To further elucidate the pH effect on the cohesive behavior of the hydrogels, SEM was used to provide a detailed description of the surface and interior morphology. As shown in Fig. S19 (ESI†), image analysis of SEM data revealed different pore sizes and shapes depending on the pH of the crosslinking system. As the pH increased from 3.5 to 8.0, the interconnected pores changed from a loose and irregular structure to a compact and rigid one for the Fe^{3+}-induced HA-Cat gels and the $NaIO_4$-induced HA-Cat gels (Fig. S19a, b, d and e, ESI†). For the HA-Cat & HA-SH gels and the HA-Cat & HA-NH_2 gels, a smooth morphological structure without any pores was observed at pH 3.5 (Fig. S19g and j, ESI†), which was because these two systems remain liquid at acidic pH. A compact and rigid porous morphological structure appeared when the pH was increased to 8.0 (Fig. S19h and k, ESI†). All of these morphological changes indicate an enhanced cohesive ability with increasing pH, which corresponds to the gelation time and mechanical strength variations. However, an inhomogeneous and rough morphological gel structure with few pores was observed when the pH was increased to 10.0 (Fig. S19c, f, i and l, ESI†). This weakened cohesive ability is due to the inhomogeneous gelation induced by a pH that is too high, which is similar to the decrease in the mechanical strength. Coincidentally, the overall picture of the interconnected pore changes was similar to the overall variation in the mechanical strength (bell-shaped curve).

2.7 Mimicking the extrusion molding process of mussel byssus

A typical mussel byssus formation process begins with the secretion of a liquid protein mixture (acidic pH) from the mussel foot gland; then, the mixture contacts seawater (slightly basic), undergoes fast solidification, and turns into a stable attachment.[8,29,32] The entire process is similar to the polymer extrusion molding. By utilizing a similar strategy, four different catechol-related reaction systems were tested, as shown in Fig. 8. A major objective of this test is to mimic the acidic-to-basic pH switch in our synthetic system, leading to gel networks and then to elucidate which crosslinking mechanism might be responsible for the rapid solidification of the mussel byssus. When the solution pH was regulated at pH 3.5, only the Fe^{3+}-induced HA-Cat system possessed limited formability, while the other three systems did not show any formability (Fig. 8, up). This result is consistent with the results of our gelation time test, in which the Fe^{3+}-induced HA-Cat system possessed rapid gelation ability (gelation time: 160 s), even at acidic pH. By increasing the solution pH to 8.0, all the pre-molding crosslinking systems exhibited good formability except for the HA-Cat & HA-NH_2 crosslinking system (Fig. 8, down), whose gelation rate was very slow (pH: 8.0, gelation time: 1700 s). Therefore, the rapid solidification process of mussel byssus might be due to a multiple crosslinking network system, including metal–catechol coordination, quinone–catechol dismutation, and quinone–thiol Michael addition reactions. These crosslinking reactions are considered the basis of the rapid solidification of secreted mussel foot proteins into hardened mussel byssus.

2.8 Self-healing ability of the different hydrogels

Marine mussels can utilize their byssus to affix themselves to rocks and thereby decrease the turbulent buffeting of the intertidal zone. Survival in this environment requires a great capacity for self-healing to avoid the catastrophic fracture.[3,7]

Fig. 8 Macroscopic images of the pre-molding mixture following extrusion into Tris–HCL buffer (pH: 3.5 up, pH: 8.0 down). Pre-molding Fe^{3+}-induced HA-Cat gel solution mixture (a), pre-molding $NaIO_4$-induced HA-Cat gel solution mixture (b), pre-molding HA-Cat & HA-SH gel solution mixture (c), pre-molding HA-Cat & HA-NH_2 gel solution mixture (d).

What type of chemistry might be involved in this self-recovery function? To answer this question, a qualitative and quantitative self-healing test was performed. Initially, qualitative tests of the self-healing property were performed by forcing a pH 8.0 gel to fracture using a spatula (Fig. 9). Second, the two gel pieces were brought together and allowed to restore the broken bonds for 100 s. As can be seen, only the Fe^{3+}-induced HA-Cat gels and the HA-Cat & HA-NH_2 gels could recover to their original shape instantly (Movie S1–S4, ESI†). Furthermore, the self-healing properties were also investigated quantitatively using rheological methods. Specifically, the hydrogels were subjected to increasing strain until they were fractured and were then allowed to heal at 0% strain for 100 s. Later, the recovery of their mechanical properties was identified as a function of time. As shown in Fig. 9, the Fe^{3+}-induced HA-Cat gels and the HA-Cat & HA-NH_2 gels instantly recovered to their original stiffness (storage modulus G' of ~380 Pa and 30 Pa, respectively), but the recovery of $NaIO_4$-induced HA-Cat gels and HA-Cat & HA-SH gels occurred slowly and was incomplete even when the healing time was prolonged. In general, the different self-healing behavior of the gels is likely due to the underlying internal crosslinking mechanism. Currently, the self-healing crosslinking mechanism is based on dynamic covalent bonds or noncovalent bonds.[39–42] The excellent self-healing behavior of the Fe^{3+}-induced HA-Cat gel is attributed to its reversible Fe^{3+}–catechol coordination bonds, which endow the gel with mussel byssus recovery ability after stress. In addition, the underlying crosslinking mechanism of the $NaIO_4$-induced HA-Cat gels and HA-Cat & HA-SH gels involved irreversible covalent bonds, making these gels unlikely to self-recover after being fractured. However, the rapid self-healing behavior of the HA-Cat & HA-NH_2 gels was unexpected, as their internal crosslinking mechanism is derived from the occurrence of Michael addition reactions or Schiff base reactions between amine and catechol groups. A Schiff base has a typical dynamic covalent bond that could be utilized for the construction of self-healing hydrogels.[15,41–43] However, under these conditions, the Schiff base was directly conjugated with benzene, which maintains its stability. According to previous research, a possible reason is the noncovalent, reversible hydrogen bonding and cation–π interactions between the catechol moiety and amine groups. The cation–π interaction is a general, noncovalent binding force comparable to hydrogen bonding in strength and has been considered a contributor to the self-healing property of mussel byssus.[43,44]

2.9 pH influence on the bulk adhesion ability of different hydrogels

Marine mussels utilize their byssus, a bioadhesive system, to affix themselves to virtually all types of inorganic and organic surfaces. Similar to commercial glue, the formation of a byssus requires both cohesive and adhesive properties.[6,45–47] Good glue balances the interplay between cohesion and adhesion. As one can imagine, there are still many unknowns regarding how to regulate these different compositions to achieve an optimized balance between cohesion and adhesion as in mussel byssus formation. What type of chemistry might be involved in the byssus crosslinking process to form good glue?

To answer this question, a lap shear test was performed. A typical adhesion test set up is depicted in Fig. S20 (ESI†). Four different catechol-related crosslinking systems were tested on virtually all types of material surfaces: metals (Al, Ti, and stainless steel), oxides (SiO_2), ceramics (glass), and synthetic polymers (PTFE, PU, PE, PC, and PS). As shown in Fig. 10a, the adhesion strength of the Fe^{3+}-induced HA-Cat gels decreased dramatically with increasing pH from 3.5 to 8.0, a consequence of catechol oxidation at a higher pH, supporting the typical notion that oxidation is detrimental to adhesion strength.

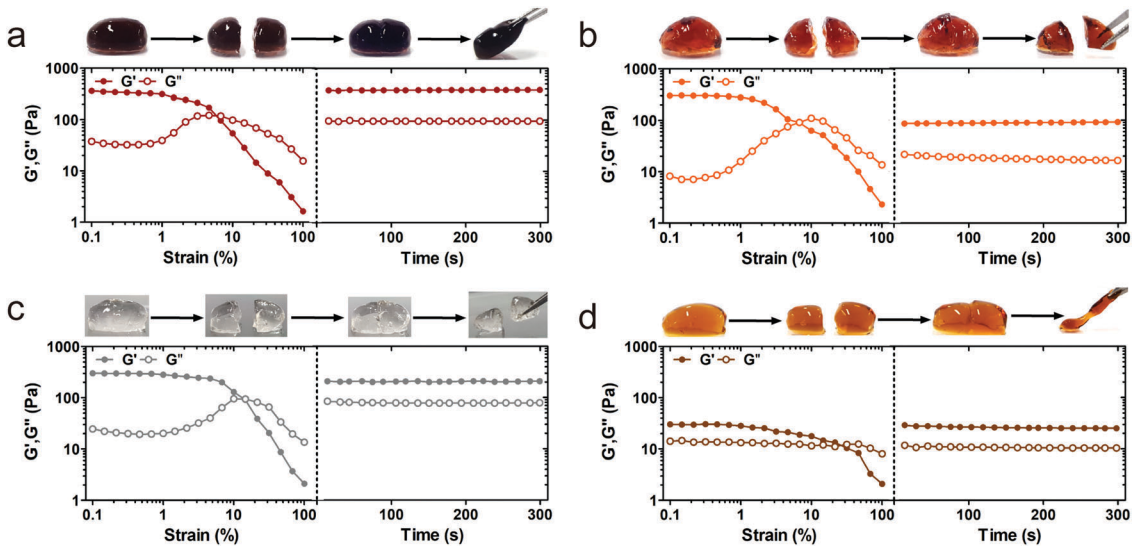

Fig. 9 Qualitative and quantitative self-healing test of Fe^{3+}-induced HA-Cat gels at pH 8.0 (a), $NaIO_4$-induced HA-Cat gels at pH 8.0 (b), HA-Cat & HA-SH gels at pH 8.0 (c), HA-Cat & HA-NH_2 gels at pH 8.0 (d). Gels were subjected to increasing strain until they were fractured followed by recovery under 0% strain for 100 s, and then monitoring by oscillatory time sweep.

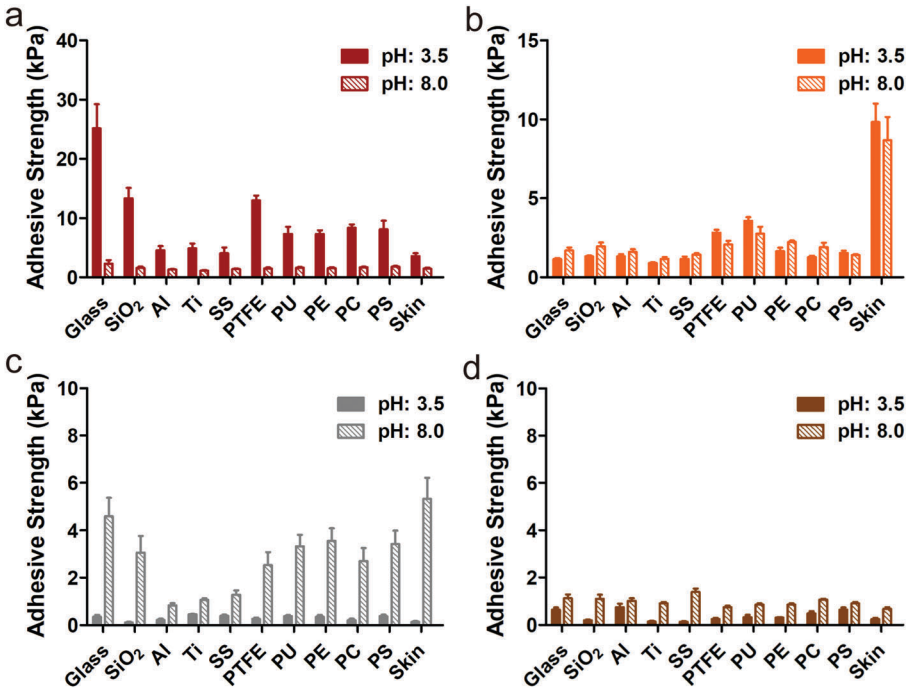

Fig. 10 Adhesion strength of the prepared adhesives (at pH: 3.5 or 8.0) on different materials. The lap shear strength of the adhesives was obtained by dividing recorded maximum load (N) by overlapped porcine surface area (m^2), giving the adhesive strength in Pascals (Pa = N m^{-2}). The test of Fe^{3+}-induced HA-Cat gels (a), $NaIO_4$-induced HA-Cat gels (b), HA-Cat & HA-SH gels (c), HA-Cat & HA-NH_2 gels (d).

However, there was no obvious variation observed during the pH increase for the $NaIO_4$-induced HA-Cat gels (Fig. 10b). The reason for this observation could be that the addition of $NaIO_4$, a potent oxidizer, diminished the effect of pH-induced oxidation. Unlike the former two gels, the HA-Cat & HA-SH gels and the HA-Cat & HA-NH_2 gels possess a limited cohesion ability, especially at low pH (pH: 3.5), which leads to a weak bulk adhesion performance (Fig. 10c and d). Once the pH was increased to 8.5, the adhesion strength was enhanced immediately due to the pH-initiated cohesion process. These results indicated that pH is a key factor modulating the bulk adhesion behavior of different catechol-related crosslinking systems. Different compositions of these systems exhibited distinct responses during the identical pH increase process. Considering that there is an urgent need to develop new bioadhesive materials for medical applications, fresh porcine skin was also used as an adherent to test the adhesion strength. The results indicated that the $NaIO_4$-induced HA-Cat gels possessed the highest adhesion strength, which is attributed to the covalent crosslinking between the quinone moieties and diverse nucleophiles of the porcine skin (*e.g.*, amine, thiol, and imidazole).

3. Conclusions

Bioinspired design is a fascinating strategy increasingly being explored in advanced materials engineering. The pH increase is a noticeable phenomenon during the mussel byssus secretion and formation processes. What type of role does pH play? By mimicking the acidic-to-basic pH switch that occurs during byssus formation, four different kinds of hyaluronic acid (HA) hydrogels (1: Fe^{3+}-induced HA-Cat hydrogels; 2: $NaIO_4$-induced HA-Cat hydrogels; 3: HA-Cat & HA-SH hydrogels; 4: HA-Cat & HA-NH_2 hydrogels) were fabricated by utilizing the multifaceted nature of catechol chemistry, including metal–catechol coordination, quinone–catechol dismutation, quinone–amine Michael addition and Schiff base reactions, or quinone–thiol Michael addition reactions (Scheme 1). The redox transition of catechol with changes in pH plays a central role in regulating the cohesion and adhesion behavior of the hydrogel system. The relationship between pH and mechanical strength (bell-shaped curve) also sheds light on how organisms can exploit a given environment (seawater pH: 8.0–8.5) to acquire the best survival ability. And this biomimetic strategy also demonstrates alternative and tunable crosslinking approaches that can overcome the limitations of current HA hydrogels. Careful management of the pH and composition affords access to a broad spectrum of HA hydrogel cohesion and adhesion properties.

Conflicts of interest

The authors declare no competing financial interest.

Acknowledgements

This work was funded by the projects of Fundamental Research of Shenzhen (JCYJ20170412101508433, JCYJ20160509154841455 and JCYJ20160509154951210).

References

1 P. Fratzl, *J. R. Soc., Interface*, 2007, **4**, 637–642.
2 M. Antonietti and P. Fratzl, *Macromol. Chem. Phys.*, 2010, **211**, 166–170.
3 M. J. Harrington, A. Masic, N. Holten-Andersen, J. H. Waite and P. Fratzl, *Science*, 2010, **328**, 216–220.
4 R. N. Martinez, S. Das, Y. Kaufman, J. N. Israelachvili and J. H. Waite, *Biofouling*, 2015, **31**, 221–227.
5 J. H. Waite, N. H. Andersen, S. Jewhurst and C. J. Sun, *J. Adhes.*, 2005, **81**, 297–317.
6 R. J. Stewart, T. C. Ransom and V. Hlady, *J. Polym. Sci., Part B: Polym. Phys.*, 2011, **49**, 757–771.
7 J. J. Wilker, *Angew. Chem., Int. Ed.*, 2010, **49**, 8076–8078.
8 B. P. Lee, P. B. Messersmith, J. N. Israelachvili and J. H. Waite, *Annu. Rev. Mater. Res.*, 2011, **41**, 99–132.
9 D. G. DeMartini, J. M. Errico, S. Sjoestroem, A. Fenster and J. H. Waite, *J. R. Soc., Interface*, 2017, **14**, 20170151.
10 J. Yu, W. Wei, E. Danner, R. K. Ashley, J. N. Israelachvili and J. H. Waite, *Nat. Chem. Biol.*, 2011, **7**, 588–590.
11 C. E. Brubaker, H. Kissler, L. Wang, D. B. Kaufman and P. B. Messersmith, *Biomaterials*, 2010, **31**, 420–427.
12 J. H. Ryu, Y. Lee, W. H. Kong, T. G. Kim, T. G. Park and H. Lee, *Biomacromolecules*, 2011, **12**, 2653–2659.
13 C. A. Del Grosso, T. W. McCarthy, C. L. Clark, J. L. Cloud and J. J. Wilker, *Chem. Mater.*, 2016, **28**, 6791–6796.
14 D. E. Fullenkamp, J. G. Rivera, Y. Gong, K. H. A. Lau, L. He, R. Varshney and P. B. Messersmith, *Biomaterials*, 2012, **33**, 3783–3791.
15 L. Li, B. Yan, J. Yang, L. Chen and H. Zeng, *Adv. Mater.*, 2015, **27**, 1294–1299.
16 B. K. Ahn, D. W. Lee, J. N. Israelachvili and J. H. Waite, *Nat. Mater.*, 2014, **13**, 867–872.
17 M. N. Collins and C. Birkinshaw, *Carbohydr. Polym.*, 2013, **92**, 1262–1279.
18 K. Y. Lee and D. J. Mooney, *Chem. Rev.*, 2001, **101**, 1869–1880.
19 L. Bian, M. Guvendiren, R. L. Mauck and J. A. Burdick, *Proc. Natl. Acad. Sci. U. S. A.*, 2013, **110**, 10117–10122.
20 J. A. Burdick and G. D. Prestwich, *Adv. Mater.*, 2011, **23**, H41–H56.
21 C. B. Highly, G. D. Prestwich and J. A. Burdick, *Curr. Opin. Biotechnol.*, 2016, **40**, 35–40.
22 L. Bian, C. Hou, E. Tous, R. Rai, R. L. Mauck and J. A. Burdick, *Biomaterials*, 2013, **34**, 413–421.
23 S. K. Seidlits, Z. Z. Khaing, R. R. Petersen, J. D. Nickels, J. E. Vanscoy, J. B. Shear and C. E. Schmidt, *Biomaterials*, 2010, **31**, 3930–3940.
24 J. Shin, J. S. Lee, C. Lee, H. Park, K. Yang, Y. Jin, J. H. Ryu, K. S. Hong, S. Moon, H. Chung, H. S. Yang, S. H. Um, J. Oh, D. Kim, H. Lee and S. Cho, *Adv. Funct. Mater.*, 2015, **25**, 3814–3824.
25 J. Lee, K. Chang, S. Kim, V. Gite, H. Chung and D. Sohn, *Macromolecules*, 2016, **49**, 7450–7459.
26 P. Bulpitt and D. Aeschlimann, *J. Biomed. Mater. Res.*, 1999, **47**, 152–169.
27 X. Zhao, *Soft Matter*, 2014, **10**, 672–687.
28 A. Ghadban, A. S. Ahmed, Y. Ping, R. Ramos, N. Arfin, B. Cantaert, R. V. Ramanujan and A. Miserez, *Chem. Commun.*, 2016, **52**, 697–700.
29 D. G. Barrett, D. E. Fullenkamp, L. He, N. Holten-Andersen, K. Y. C. Lee and P. B. Messersmith, *Adv. Funct. Mater.*, 2013, **23**, 1111–1119.
30 Z. Guo, K. Ni, D. Wei and Y. Ren, *RSC Adv.*, 2015, **5**, 37377–37384.
31 D. E. Fullenkamp, D. G. Barrett, D. R. Miller, J. W. Kurutz and P. B. Messersmith, *RSC Adv.*, 2014, **4**, 25127–25134.
32 N. Holten-Andersen, M. J. Harrington, H. Birkedal, B. P. Lee, P. B. Messersmith, K. Y. C. Lee and J. H. Waite, *Proc. Natl. Acad. Sci. U. S. A.*, 2011, **108**, 2651–2655.
33 X. Xu, A. K. Jha, D. A. Harrington, M. C. Farach-Carson and X. Jia, *Soft Matter*, 2012, **8**, 3280–3294.
34 M. Bisaglia, S. Mammi and L. Bubacco, *J. Biol. Chem.*, 2007, **282**, 15597–15605.
35 C. A. Del Grosso, T. W. McCarthy, C. L. Clark, J. L. Cloud and J. J. Wilker, *Chem. Mater.*, 2016, **28**, 6791–6796.
36 E. Herlinger, R. F. Jameson and W. Linert, *J. Chem. Soc., Perkin. Trans. 2*, 1995, 259–263.
37 J. Yang, M. A. C. Stuart and M. Kamperman, *Chem. Soc. Rev.*, 2014, **43**, 8271–8298.
38 D. R. Miller, J. E. Spahn and J. H. Waite, *J. R. Soc., Interface*, 2015, **12**, 20150614.
39 B. K. Ahn, D. W. Lee, J. N. Israelachvili and J. H. Waite, *Nat. Mater.*, 2014, **13**, 867–872.
40 Z. Wei, J. H. Yang, Z. Q. Liu, F. Xu, J. X. Zhou, M. Zrínyi, Y. Osada and Y. M. Chen, *Adv. Funct. Mater.*, 2015, **25**, 1352–1359.
41 Y. Zhang, L. Tao, S. Li and Y. Wei, *Biomacromolecules*, 2011, **12**, 2894–2901.
42 Y. Zhang, B. Yang, X. Zhang, L. Xu, L. Tao, S. Li and Y. Wei, *Chem. Commun.*, 2012, **48**, 9305.
43 X. Zhao, M. Zhang, B. Guo and P. X. Ma, *J. Mater. Chem. B*, 2016, **4**, 6644–6651.
44 J. P. Gallivan and D. A. Dougherty, *Proc. Natl. Acad. Sci. U. S. A.*, 1999, **96**, 9459–9464.
45 J. J. Wilker, *Nat. Mater.*, 2014, **13**, 849–850.
46 J. Lee, K. C. Yoo, J. Ko, B. Yoo, J. Shin, S. Lee and D. Sohn, *Carbohydr. Polym.*, 2017, **164**, 309–316.
47 S. Hong, K. Yang, B. Kang, C. Lee, I. T. Song, E. Byun, K. I. Park, S. Cho and H. Lee, *Adv. Funct. Mater.*, 2013, **23**, 1774–1780.

